Supplementary Material

Ternary Metal Oxynitride $Y_2Zr_2O_{7-x}N_x$ for Selective NO_2 Electrochemical Sensing

Xichao Mo[a], Jinyang Hu[b], Zhaorui Zhang[c], Jiaxin Li[a], Chonghui Zhu[a], Congling Yin[b], Jinkui Chu[c] and Minghui Yang*[a]

[a] School of Environmental Science and Technology, Dalian University of Technology, No.2 Linggong Road, Ganjingzi District, Dalian, 116024, China

[b] MOE Key Laboratory of New Processing Technology for Nonferrous Metal and Materials, Guangxi Key Laboratory of Optical and Electronic Materials and Devices, Collaborative Innovation Center for Exploration of Nonferrous Metal Deposits and Efficient Utilization of Resources, College of Materials Science and Engineering, Guilin University of Technology, Guilin 541004, P. R. China.

[c] State Key Laboratory of High-performance Precision Manufacturing, Dalian University of Technology, Dalian 116024, China.

E-mail: myang@dlut.edu.cn

EXPERIMENTAL METHODS

Materials

All chemical reagents used in this study were of analytical grade and required no additional purification. Zirconium oxide (ZrO_2, 99.9%), yttrium nitrate hexahydrate ($Y(NO_3)_3 \cdot 6H_2O$, 99.9%), and anhydrous citric acid ($C_6H_8O_7$, 99.5%) were obtained from Aladdin Industrial Corporation. XC-72R carbon blacks, along with Nafion and the Nafion 115 membrane, were sourced from CABOT, U.S.A. Ethylene glycol ($C_2H_6O_2$, 99.0%) and methanol (CH_4O, AR) were supplied by Tianjin Fuyu Fine Chemical Co., Ltd.

The preparation procedures for all gas samples.

The testing procedure utilizes the traditional static method, where a specified volume of NO_2 is injected into a 250 mL gas collection cylinder using a syringe to achieve different gas concentrations. For example, to detect NO_2 gas, we extract 25 mL of 100 ppm NO_2 gas with a syringe, inject it into a 250 mL gas collector, and allow it to disperse evenly, yielding a 10 ppm NO_2 concentration. For selectivity testing, target gases were sourced from various 100 ppm gas cylinders, with dry nitrogen as the diluent. The test gases in the cylinders were all dry gases. Humidity testing was conducted by preparing various saturated salt solutions and placing the device above them to simulate current under different humidity conditions. The saturated salt solution bottles of LiCl, $MgCl_2$, $Mg(NO_3)_2$, NaCl, KCl, and KNO_3 resulted in relative humidities (RH) of 11%, 33%, 54%, 75%, 85%, and 95%, respectively.

Procedure for using saturated salt solution bottles: Place the sensor in a sealed volumetric bottle containing an 11% saturated salt solution, setting its current as the baseline. Then, sequentially expose the sensor to volumetric bottles with 33%, 54%, 75%, 85%, and 95% saturated salt solutions, monitoring the changes in current. If the sensor exhibits excellent humidity resistance, the current variation should be minimal. To ensure the accuracy of repeatability tests, a micro-syringe should be used to periodically inject water into the sponge on the left side of the sensor.

The calibration formula for gas concentration is detailed below.

1. Formulation of gas distribution when measuring liquid vapor

The liquid vapor injection volume (V_X) is calculated using equation (1):

$$V_X = \frac{V \times C \times M}{22.4 \times d \times p} \times 10^{-9} \times \frac{273 + T_r}{273 + T_b} (1)$$

2. Formula for gas distribution when measuring gas

The gas injection volume (V_X) is calculated using equation (2):

$$V_X = V \times C \times 10^{-6} \times \frac{273 + T_r}{273 + T_b} (2)$$

In equations (1) and (2):

V——test tank volume in milliliters (mL);

C——liquid vapor concentration in parts per million (ppm);

M——liquid molecular weight (g);

D——liquid specific gravity in grams per cubic centimeter (g/cm^3);

P——liquid purity;

Tr——room temperature, in degrees Celsius (°C);

Tb——test the temperature inside the box in degrees Celsius (°C).

EXPERIMENT AND DISCUSSION

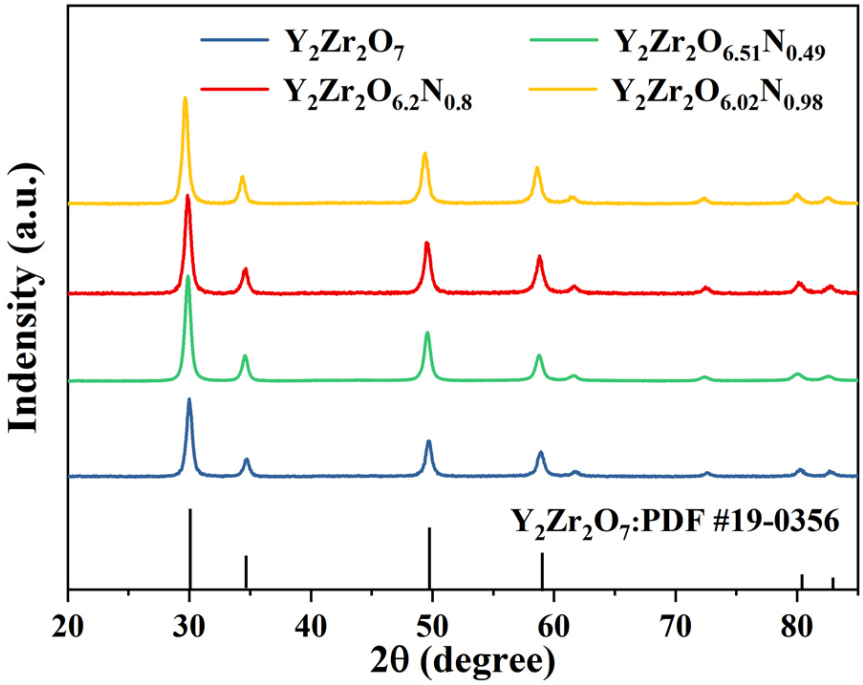

Figure S1. X-ray diffraction (XRD) patterns of $Y_2Zr_2O_7$ and $Y_2Zr_2O_{7-x}N_x$.

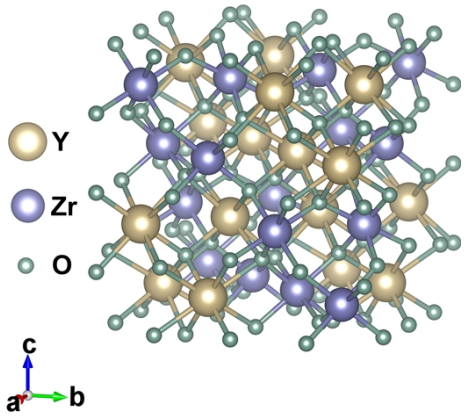

Figure S2. Refined molecular structure of $Y_2Zr_2O_7$.

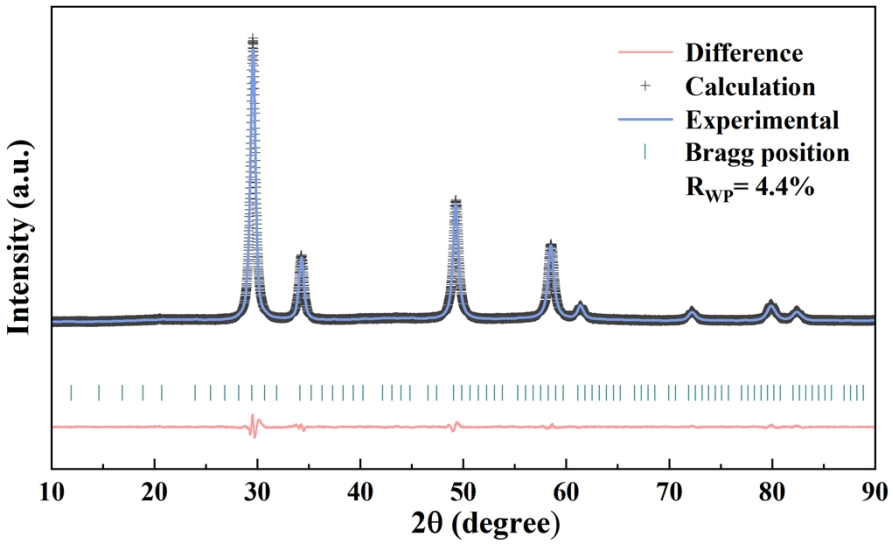

Figure S3. The Rietveld fitted powder X-ray diffraction pattern of $Y_2Zr_2O_7$.

Table S1

Refined Structural Parameters of $Y_2Zr_2O_7$.

Atom	Site	*x, y, z*	Beq	Occupancy
Y	16d	0.5, 0.5, 0.5	1.395	1
Zr	16c	0, 0, 0	1.395	1
O1	48f	0.3617, 0.1250, 0.1250	0.710	1
O2	8b	0.3750, 0.3750, 0.3750	0.710	1

$a = b = c$ = 10.473(1) Å

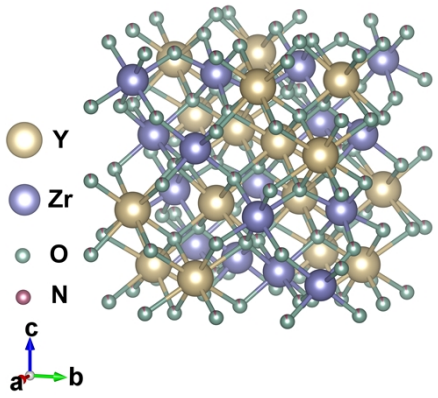

Figure S4. Refined molecular structure of $Y_2Zr_2O_{6.51}N_{0.49}$.

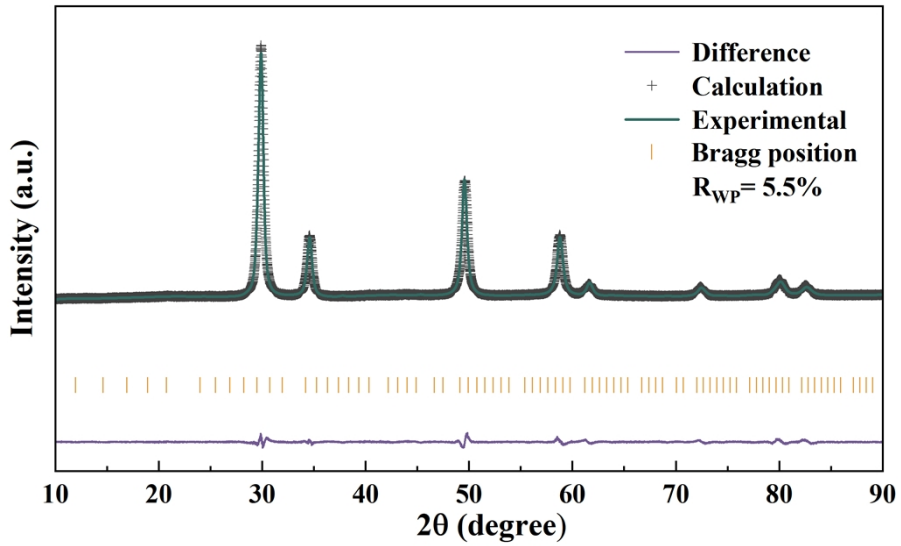

Figure S5. The Rietveld fitted powder X-ray diffraction pattern of $Y_2Zr_2O_{6.51}N_{0.49}$.

Table S2

Refined Structural Parameters of $Y_2Zr_2O_{6.51}N_{0.49}$.

Atom	Site	*x, y, z*	Beq	Occupancy
Y	16d	0.5, 0.5, 0.5	2.300	1
Zr	16c	0, 0, 0	1.550	1
O1	48f	0.3417, 0.1250, 0.1250	1	0.93
O2	8b	0.3750, 0.3750, 0.3750	1.3	0.93
N1	48f	0.3417, 0.1250, 0.1250	1	0.07
N2	8b	0.3750, 0.3750, 0.3750	1.3	0.07

$a = b = c = 10.491(1)$ Å

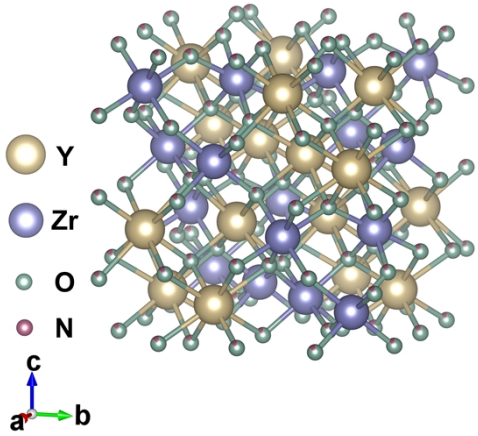

Figure S6. Refined molecular structure of $Y_2Zr_2O_{6.02}N_{0.98}$.

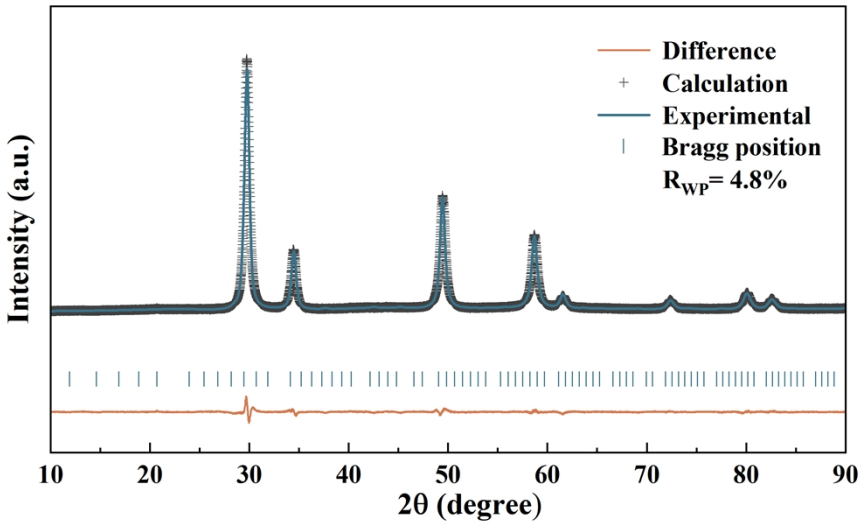

Figure S7. The Rietveld fitted powder X-ray diffraction pattern of $Y_2Zr_2O_{6.02}N_{0.98}$.

Table S3

Refined Structural Parameters of $Y_2Zr_2O_{6.02}N_{0.98}$.

Atom	Site	*x, y, z*	Beq	Occupancy
Y	16d	0.5, 0.5, 0.5	0.85	1
Zr	16c	0, 0, 0	0.76	1
O1	48f	0.3417, 0.1250, 0.1250	2.61	0.859
O2	8b	0.3750, 0.3750, 0.3750	2.2	0.859
N1	48f	0.3587, 0.1250, 0.1250	2.61	0.14
N2	8b	0.3750, 0.3750, 0.3750	2.2	0.14

$a = b = c$ = 10.473(5) Å

Table S4

Refined Structural Parameters of $Y_2Zr_2O_{6.2}N_{0.8}$.

Atom	Site	*x, y, z*	Beq	Occupancy
Y	16d	0.5, 0.5, 0.5	0.32	1
Zr	16c	0, 0, 0	0.59	1
O1	48f	0.3417, 0.1250, 0.1250	2.39	0.885
O2	8b	0.3750, 0.3750, 0.3750	2.1	0.885
N1	48f	0.3417, 0.1250, 0.1250	2.39	0.115
N2	8b	0.3750, 0.3750, 0.3750	2.1	0.115

$a = b = c = 10.470(3)$ Å

Table S5

N, O element analysis test

Sample	Weight (mg)	N (%)	O (%)	Occupancy (N/(O+N)%)	x	stoichiometric ratio ($Y_2Zr_2O_{7-x}N_x$)
$Y_2Zr_2O_{6.51}N_{0.49}$	2.813	0.13	1.72	7.027	0.49	$Y_2Zr_2O_{6.51}N_{0.49}$
$Y_2Zr_2O_{6.2}N_{0.8}$	2.972	0.2	1.54	11.494	0.8	$Y_2Zr_2O_{6.2}N_{0.8}$
$Y_2Zr_2O_{6.02}N_{0.98}$	2.917	0.26	1.49	14.054	0.98	$Y_2Zr_2O_{6.02}N_{0.98}$

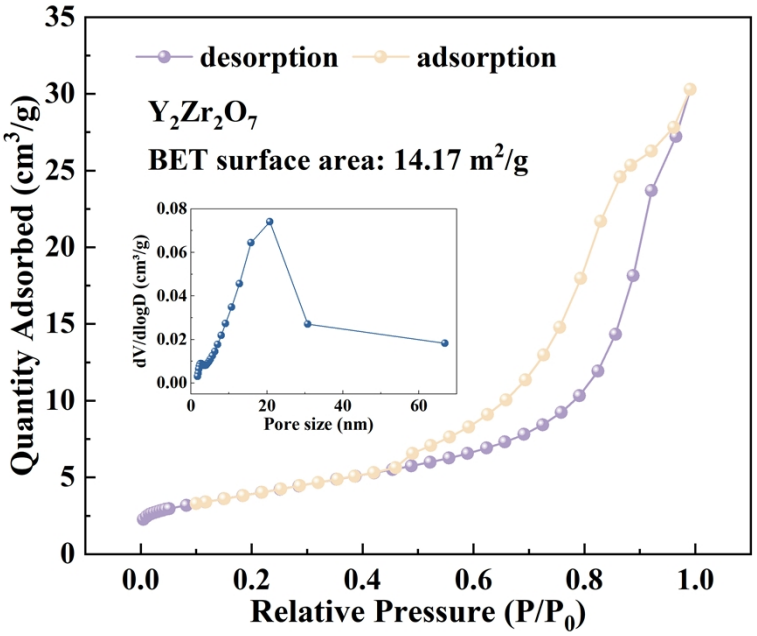

Figure S8. N_2 sorption isotherms and Brunauer Emmett Teller (BET) surface area of $Y_2Zr_2O_7$.

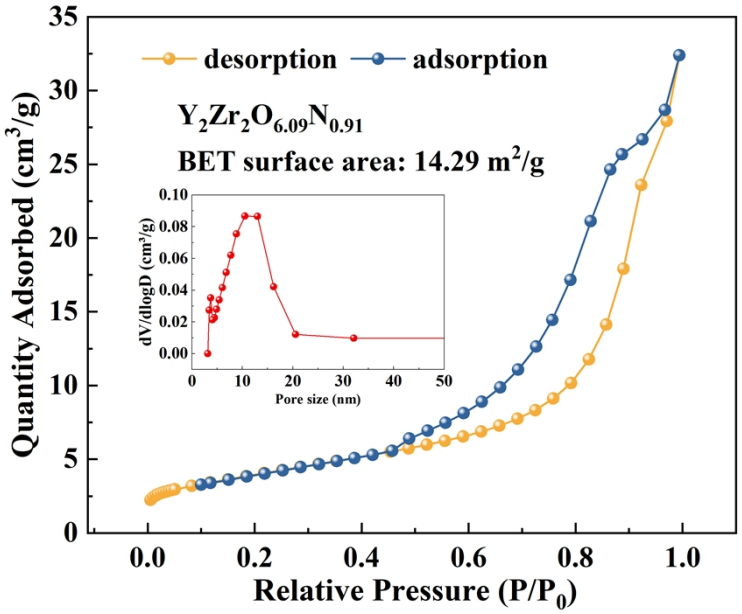

Figure S9. N_2 sorption isotherms and Brunauer Emmett Teller (BET) surface area of $Y_2Zr_2O_{6.2}N_{0.8}$.

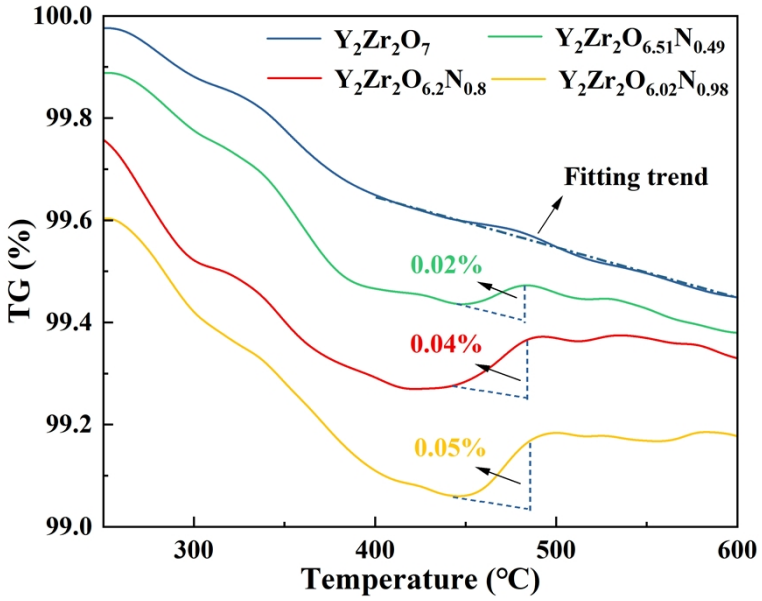

Figure S10. Thermogravimetric (TGA) testing of $Y_2Zr_2O_7$ and $Y_2Zr_2O_{7-x}N_x$ samples.

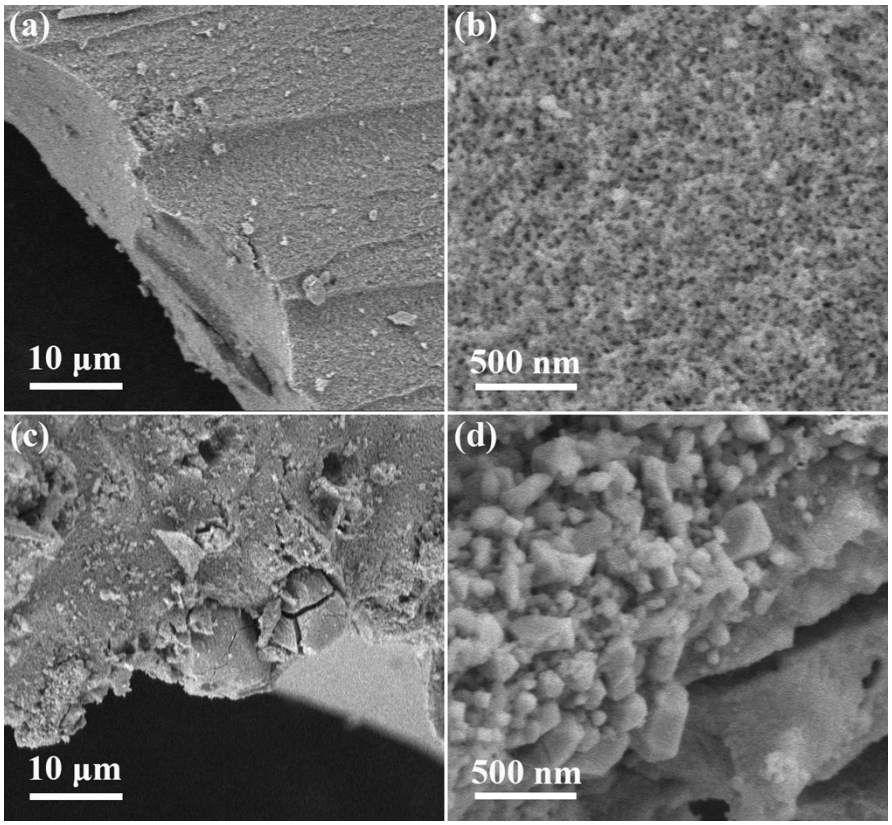

Figure S11. Scanning electron microscope (SEM) images of (a), (b) $Y_2Zr_2O_7$ and (c), (d) $Y_2Zr_2O_{6.2}N_{0.8}$.

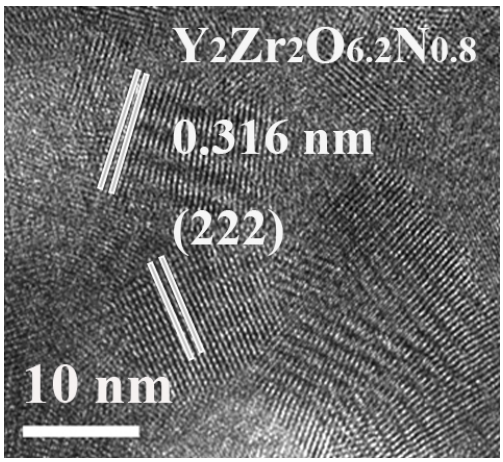

Figure S12. High-resolution transmission electron microscopy (HRTEM) image of $Y_2Zr_2O_{6.2}N_{0.8}$.

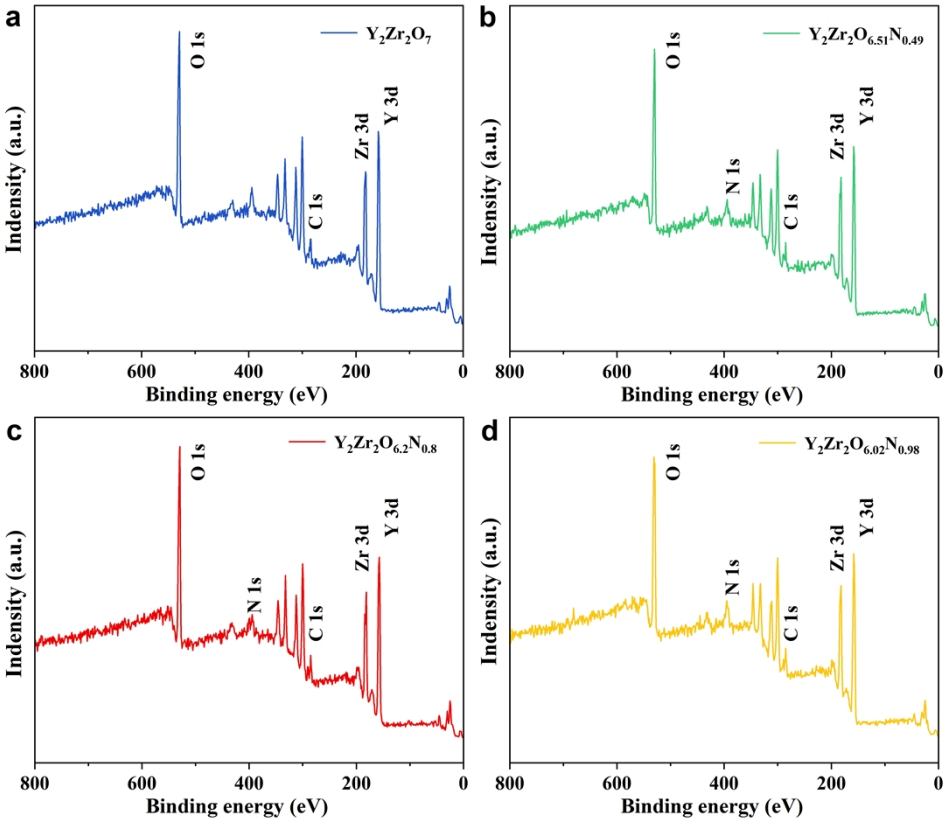

Figure S13. X-ray photoelectron spectroscopy (XPS) survey spectra of (a) $Y_2Zr_2O_7$, (b) $Y_2Zr_2O_{6.51}N_{0.49}$, (c) $Y_2Zr_2O_{6.2}N_{0.8}$ and (d) $Y_2Zr_2O_{6.02}N_{0.98}$.

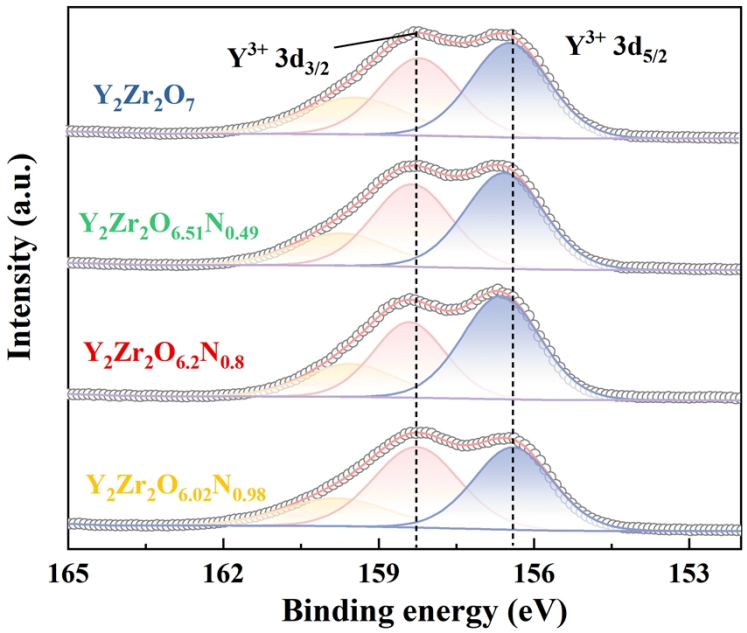

Figure S14. X-ray photoelectron spectroscopy (XPS) spectrum of $Y_2Zr_2O_7$ and $Y_2Zr_2O_{7-x}N_x$ for Y 3d.

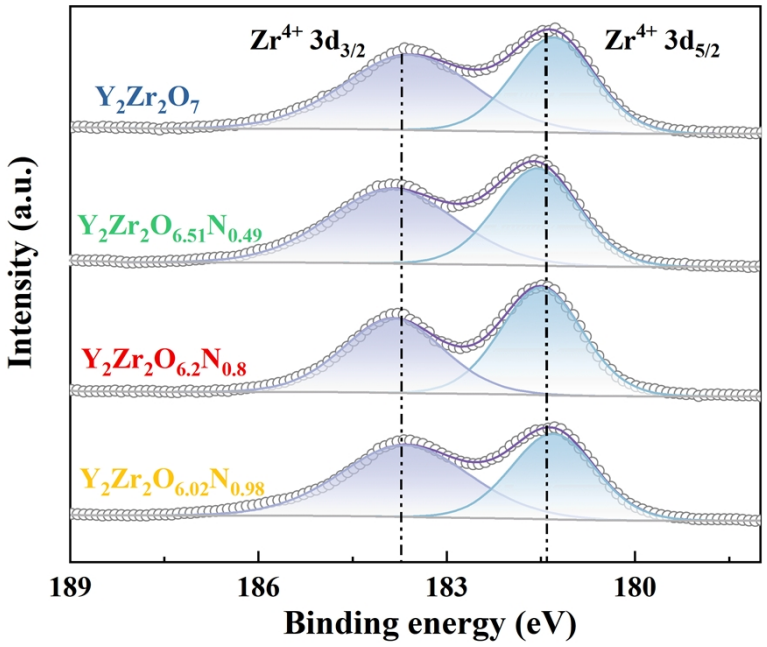

Figure S15. X-ray photoelectron spectroscopy (XPS) spectrum of $Y_2Zr_2O_7$ and $Y_2Zr_2O_{7-x}N_x$ for Zr 3d

\

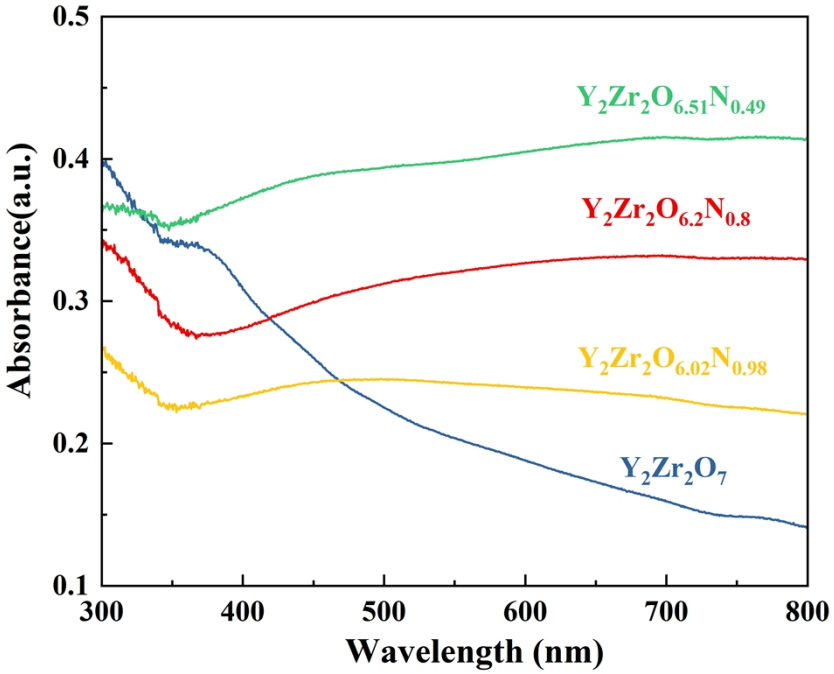

Figure S16. (a) UV–vis diffuse reflectance spectra (UV–vis–DRS) of $Y_2Zr_2O_7$ and $Y_2Zr_2O_{7-x}N_x$.

Figure S17. The digital photograph of samples prepared with different nitriding time of $Y_2Zr_2O_7$ (ranging from 5 h to 15 h, from left to right).

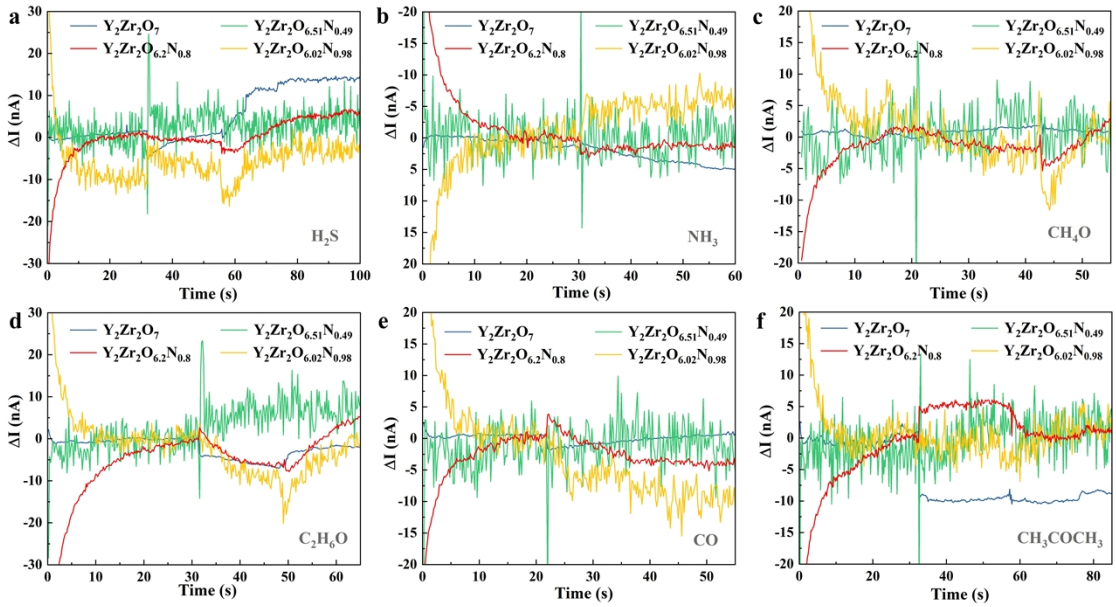

Figure S18. Selective dynamic response curve of (a) hydrogen sulfide, (b) ammonia, (c) methanol, (d) ethanol, (e) carbon monoxide and (f) acetone.

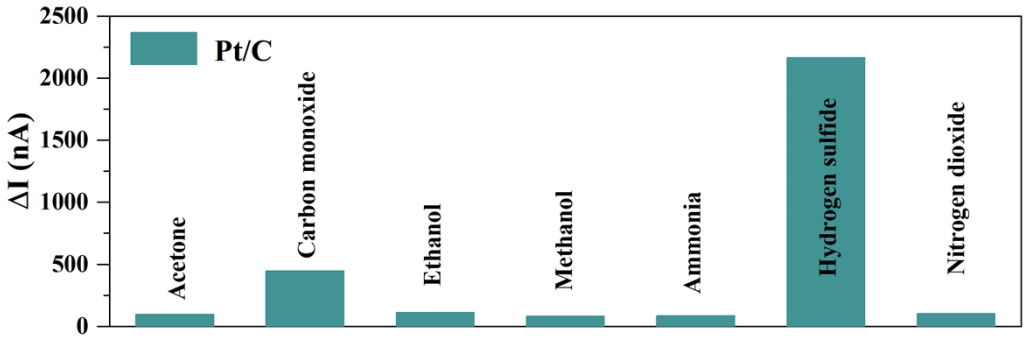

Figure S19. Selectivity of sensors toward different testing gases with a concentration of 50 ppm NO_2 and 50 ppm of other gases at room temperature.

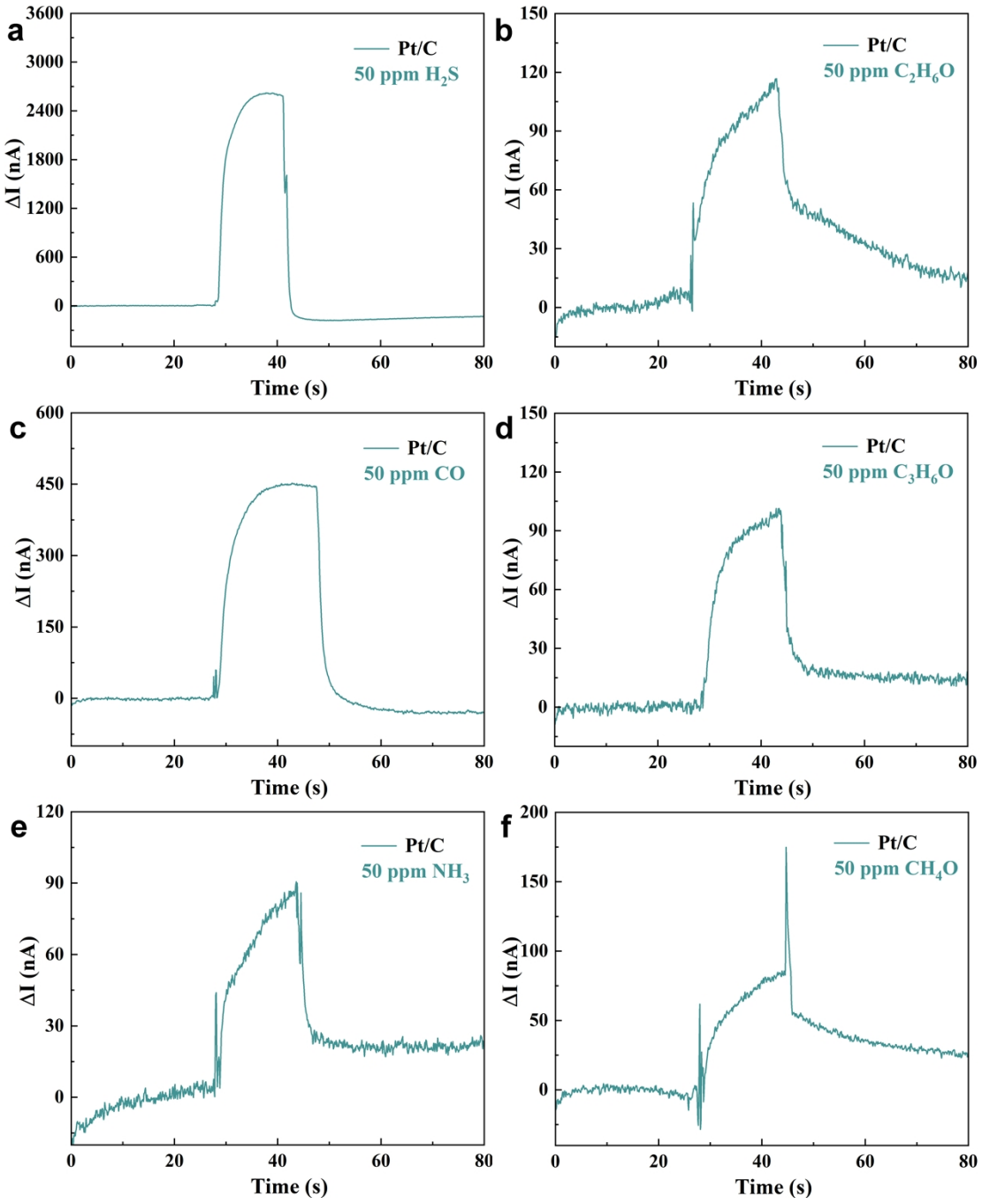

Figure S20. Selective dynamic response curve of 50 ppm (a) hydrogen sulfide, (b) ethanol, (c) carbon monoxide, (d) acetone, (e) ammonia and (f) methanol.

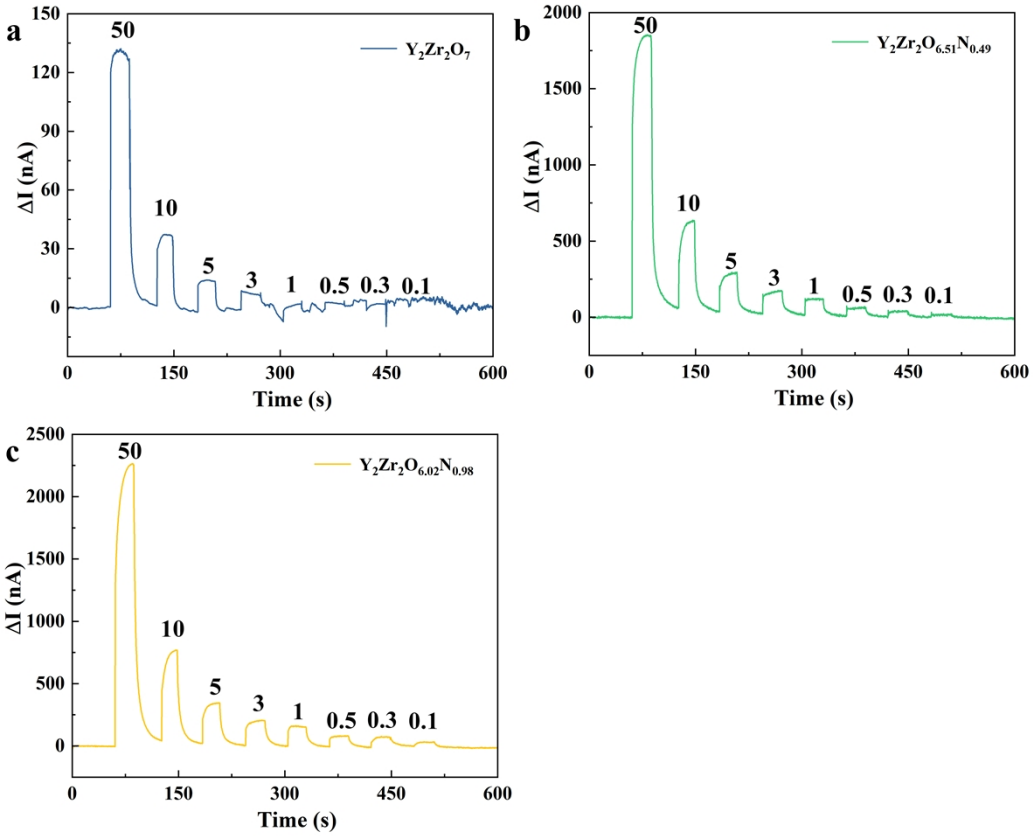

Figure S21. Dynamic gas-sensing transients of (a) $Y_2Zr_2O_7$, (b) $Y_2Zr_2O_{6.51}N_{0.49}$ and (c) $Y_2Zr_2O_{6.02}N_{0.98}$ when exposed to 50-0.1 ppm NO_2 at room temperature.

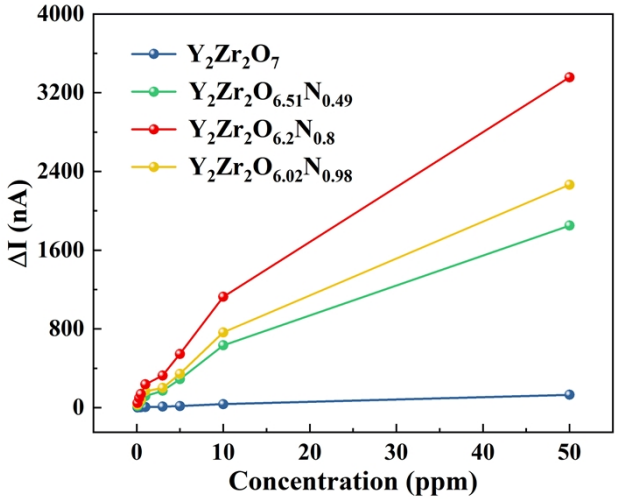

Figure S22. The relationship between response and the change of gas concentration of the sensors.

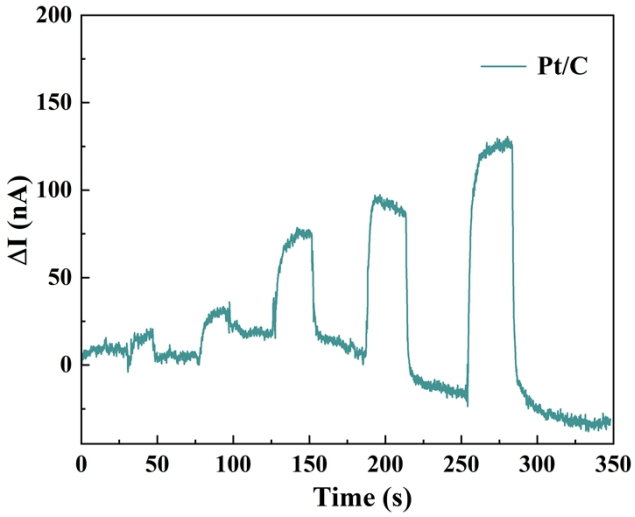

Figure S23. Dynamic gas-sensing transients of Pt/C when exposed to 5-100 ppm NO_2 at room temperature.

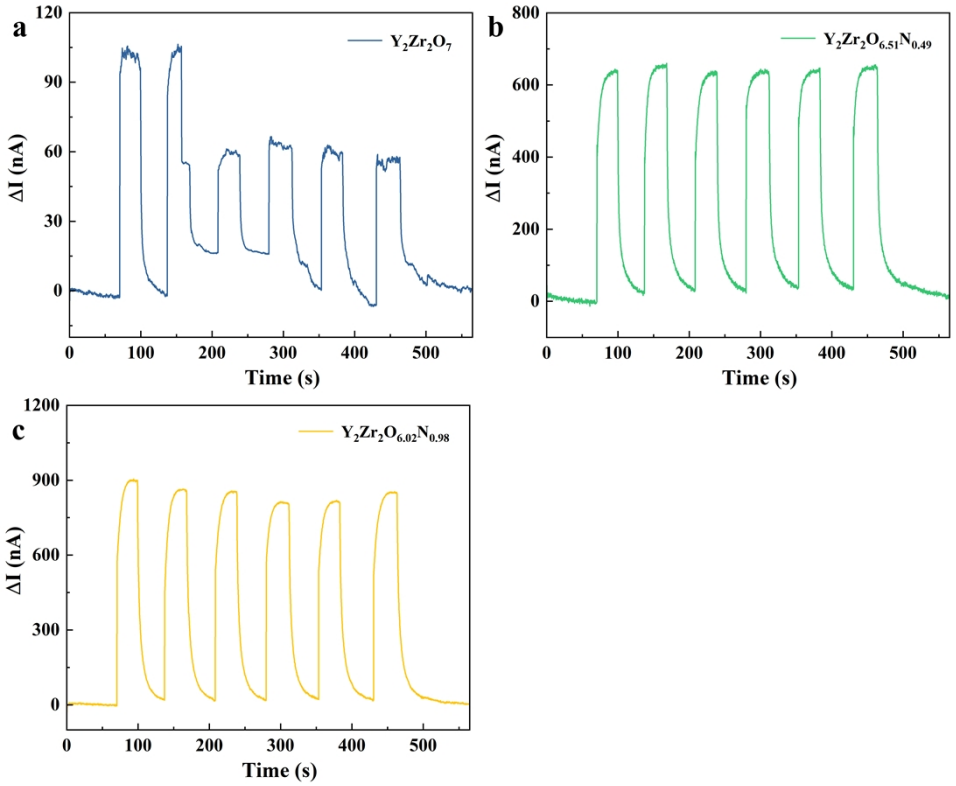

Figure S24. 6-cycle dynamic sensing response of (a) $Y_2Zr_2O_7$, (b) $Y_2Zr_2O_{6.51}N_{0.49}$ and (c) $Y_2Zr_2O_{6.02}N_{0.98}$ when exposed to 10 ppm NO_2 at room temperature.

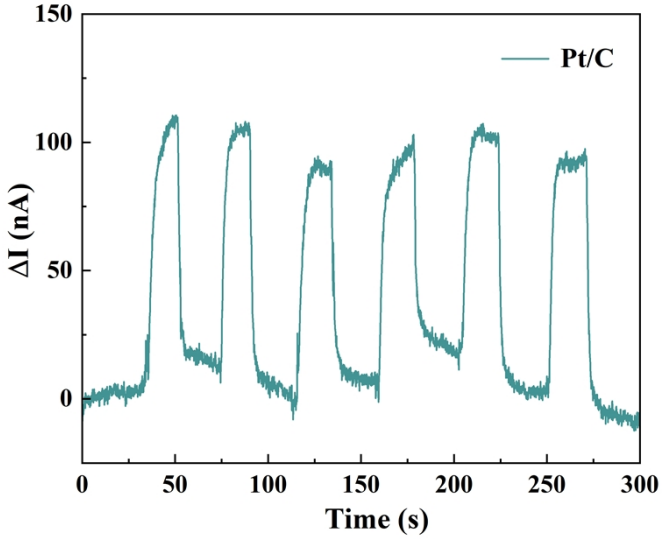

Figure S25. 6-cycle dynamic sensing response of Pt/C when exposed to 10 ppm NO_2 at room temperature.

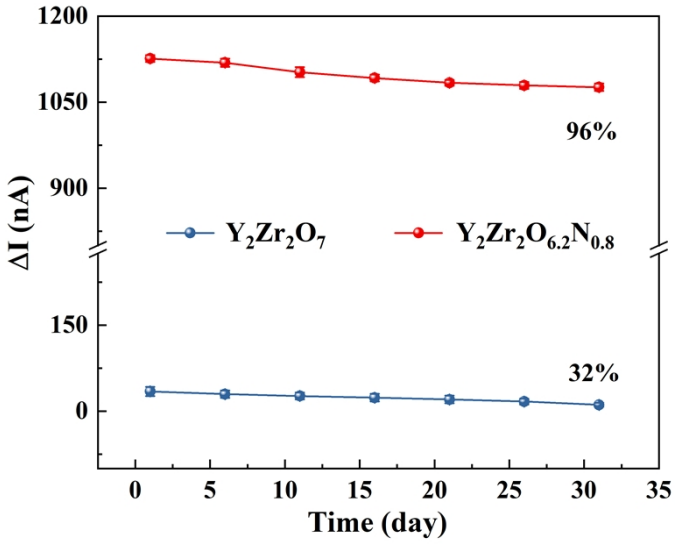

Figure S26. Long-term stability of $Y_2Zr_2O_7$ and $Y_2Zr_2O_{6.2}N_{0.8}$ toward 10 ppm NO_2.

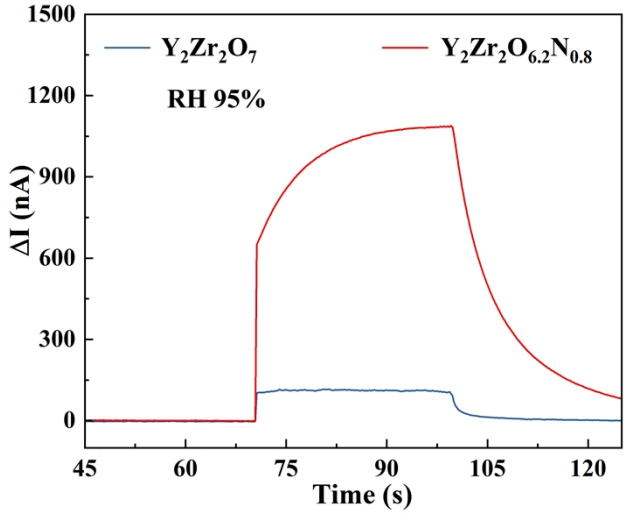

Figure S27. Response curve to 10 ppm NO_2 under 95% relative humidity conditions.

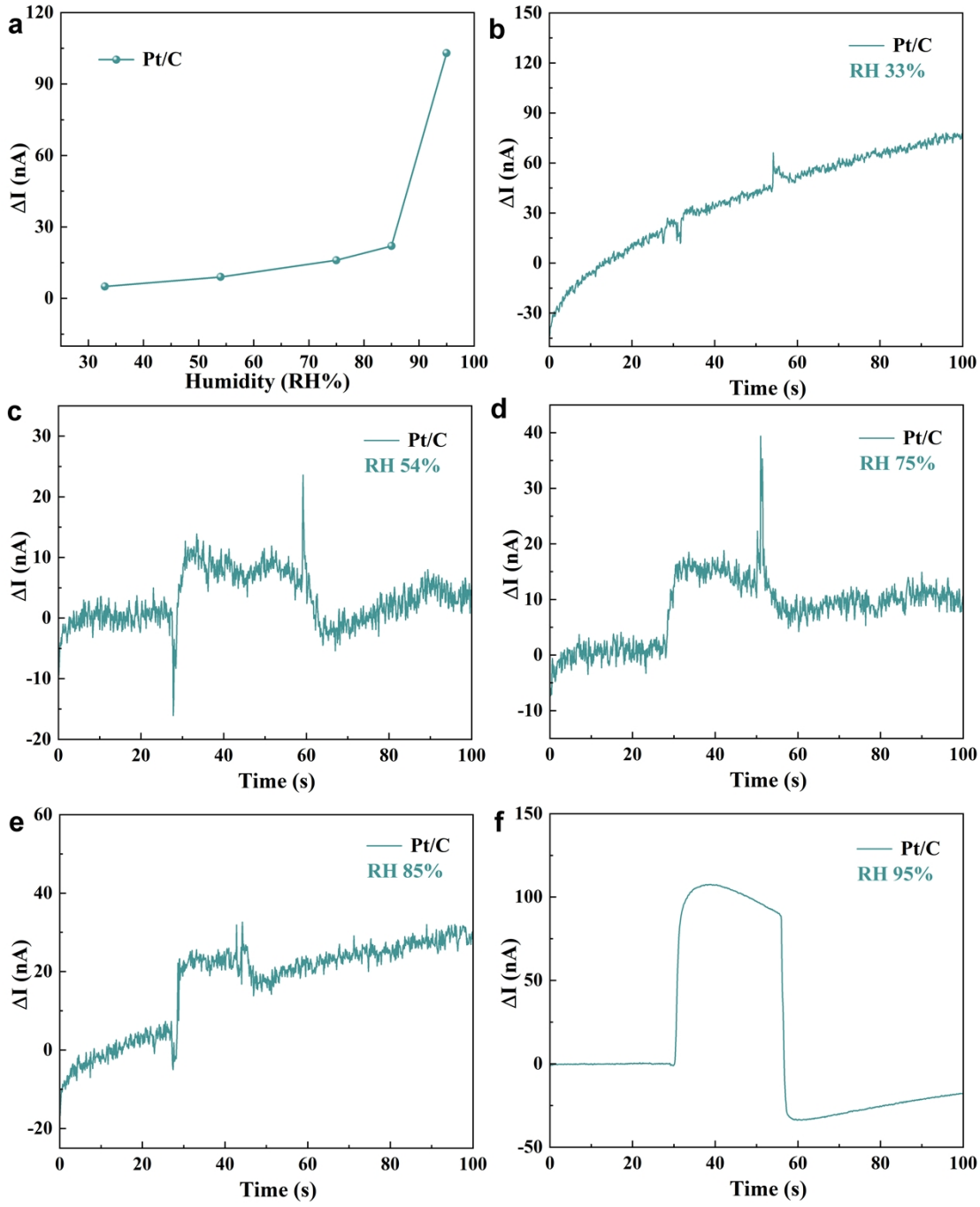

Figure S28. (a) The relationship between response and the change of humidity of the sensors. Dynamic response curve of each device under different humidity (b) 33%; (c) 54%; (d) 75%; (e) 85%; (f) 95%.

Table S6

Comparison of the Reported NO_2 Sensing Materials at room temperature

Sensing type	Sensing material	Detection range (ppm)	τ_{res}/τ_{recov} (s) Concentration	Stability 96% (days)	Tempera -ture (°C)	LOD (ppm)	Ref.
electrochemical sensor	$Y_2Zr_2O_{6.2}N_{0.8}$	0.1-10	20/20 (10 ppm)	30	RT	0.05	This work
	Pt/C	5-100	32/49 (10 ppm)	7	RT	1	This work
	MoS_2	1-50	55/55 (10 ppm)	10	RT	0.05	2*
chemiresistive sensor	PPy/N-MWCNT	0.25-9	65/668 (5 ppm)	8	RT	0.25	3
	MoS_2 p-n junction	0.1-100	150/30 (20 ppm)	9	RT	0.008	4
	$MoSe_2$	5-25	52/69 (15 ppm)	26	RT	0.041	5
	$Ti_3C_2T_X$	0.05-20	132/230 (1 ppm)	22	RT	0.05	6
	NbS_2	0.5-5	18/338 (10 ppm)	14	RT	0.2	7
	$Ti_3C_2T_X$/γ-PGA	2-50	45/16 (10 ppm)	10	RT	2	8
	Nb_2CT_X-CTAB	5-25	57/68 (15 ppm)	22	RT	0.021	9
	$Mo_2TiC_2T_X/MoS_2$	0.2-50	35/141 (50 ppm)	18	RT	0.003	10
	BSi	1-5	35/25 (4 ppm)	10	RT	0.957	11

* Currently, research on electrochemical fuel cell-type sensors for NO_2 detection is limited; therefore, a semiconductor-type NO_2 gas sensor is included for comparison.

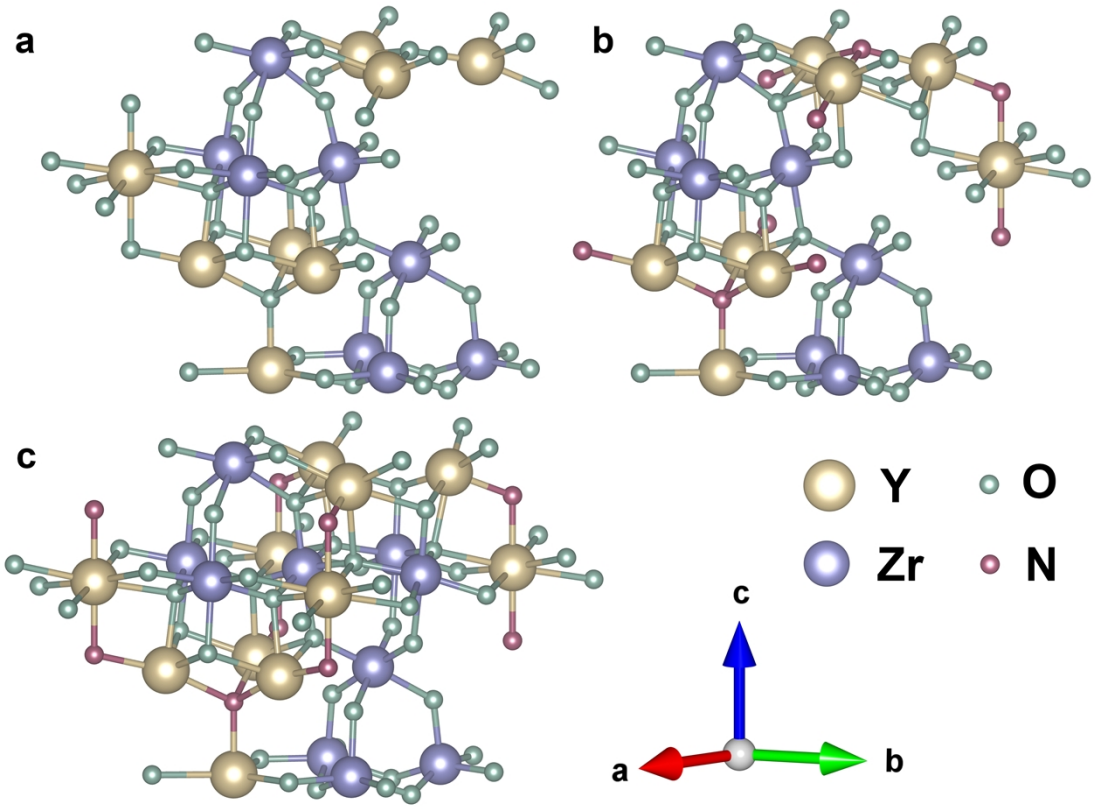

Figure S29. Molecular model of (a) YZrO; (b)YZrON and (c)YZrONV

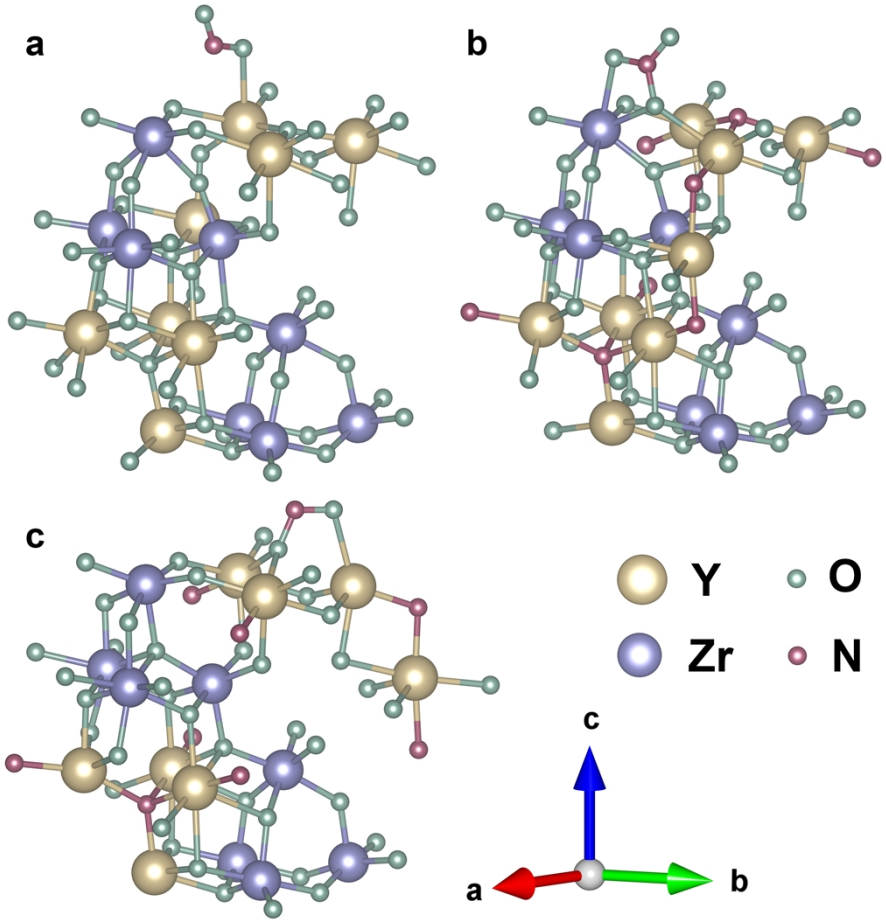

Figure S30. Structural diagram of adsorption NO_2 (a) YZrO; (b)YZrON and (c)YZrONV

Table S7

Adsorption energies and charge transferred between YZrO, YZrON and YZrONV and an adsorbed NO_2 molecule.

System	Adsorption energy (eV)	Charge transferred (|e|)
YZrO	-0.735	0.229
YZrON	-1.988	0.425
YZrONV	-3.218	0.838

References

1 X. Mo, C. Zhu, Z. Zhang, X. Yan, C. Han, J. Li, J. P. Attfield, M. Yang, *Adv. Mater.* **2024**, 36 (41), 2409294.

2 L. Huang, W. Li, H. Sun, J. Zhang, B. Wang, Q. Lu, T. Wang, X. Liang, F. Liu, P. Sun, F. Liu, G. Lu, *Sens. Actuators B: Chem.* **2024**, 399, 134808.
3 B. Liu, X. Liu, Z. Yuan, Y. Jiang, Y. Su, J. Ma, et al. *Sens. Actuators B: Chem.* **2019**, *295*, 86–92.
4 W. Zheng, Y. Xu, L. Zheng, C. Yang, N. Pinna, X. Liu, J. Zhang, *Adv. Funct. Mater.* **2020**, *30*, 2000435.
5 K. Rathi, K. Pal, *Adv. Mater. Interfaces* **2020**, *7*, 2000140.
6 Y. Song, Y. Xu, Q. Guo, Z. Hua, F. Yin, W. Yuan, *ACS Appl. Mater. Interfaces* **2021**, *13*, 39772-39780.
7 Y. Kim, K.C. Kwon, S. Kang, C. Kim, T.H. Kim, S.P. Hong, et al., *ACS Sens.* **2019**, *4*, 2395–2402.
8 Q. Zhao, D. Sun, S. Wang, Z. Duan, Z. Yuan, G. Wei, J. L. Xu, H. Tai, Y. Jiang, *ACS Sens.* **2021**, *6*, 2858-2867.
9 K. Rathi, N. K. Arkoti, K. Pal, *Adv. Mater. Interfaces* **2022**, *9*, 2200415.
10 Q. Zhao, W. Zhou, M. Zhang, Y. Wang, Z. Duan, C. Tan, B. Liu, F. Ouyang, Z. Yuan, H. Tai, Y. Jiang, *Adv. Funct. Mater.* **2022**, *32*, 2203528.
11 G. Ayvazyan, K. Ayvazyan, L. Hakhoyan, A. Semchenko, *Phys Status Solidi Rapid Res Lett* **2023**, *17*, 2300058.